



ALMA MATER STUDIORUM
UNIVERSITÀ DI BOLOGNA

ARCHIVIO ISTITUZIONALE
DELLA RICERCA

Alma Mater Studiorum Università di Bologna Archivio istituzionale della ricerca

Evolution of drop size distribution in natural rain

This is the final peer-reviewed author's accepted manuscript (postprint) of the following publication:

Published Version:

D'Adderio, L., Porcù, F., Tokay, A. (2018). Evolution of drop size distribution in natural rain. *ATMOSPHERIC RESEARCH*, 200, 70-76 [10.1016/j.atmosres.2017.10.003].

Availability:

This version is available at: <https://hdl.handle.net/11585/621190> since: 2018-02-12

Published:

DOI: <http://doi.org/10.1016/j.atmosres.2017.10.003>

Terms of use:

Some rights reserved. The terms and conditions for the reuse of this version of the manuscript are specified in the publishing policy. For all terms of use and more information see the publisher's website.

This item was downloaded from IRIS Università di Bologna (<https://cris.unibo.it/>).
When citing, please refer to the published version.

(Article begins on next page)

This is the final peer-reviewed accepted manuscript of:

Leo Pio D'Adderio, Federico Porcù, Ali Tokay, Evolution of drop size distribution in natural rain, Atmospheric Research, Volume 200, 2018, Pages 70-76.

The final published version is available at:
<https://doi.org/10.1016/j.atmosres.2017.10.003>

Rights / License:

The terms and conditions for the reuse of this version of the manuscript are specified in the publishing policy. For all terms of use and more information see the publisher's website.

This item was downloaded from IRIS Università di Bologna (<https://cris.unibo.it/>)

When citing, please refer to the published version.

1
2
3
4
5
6
7
8
9
10
11
12
13
14
15
16
17
18
19
20
21
22

Evolution of Drop Size Distribution in natural rain

Leo Pio D'Adderio

Dep. of Physics and Earth Science, University of Ferrara, Italy,

Federico Porcù

Dep. of Physics and Astronomy, University of Bologna, Italy

Ali Tokay

JCET-University of Maryland Baltimore County and NASA-Goddard Space Flight Center, Greenbelt,

Maryland, USA.

Corresponding author: Leo Pio D'Adderio, Department of Physics and earth Science, University of Ferrara,
44122, Ferrara, Italy
Email: dadderio@fe.infn.it

23 Abstract

24 Both numerical modeling and laboratory experiments document the possibility of a raindrop size
25 distribution (DSD) to evolve to an equilibrium stage (EDSD), where all the principal processes occur
26 at steady rates.

27 The aim of this work is to observe the temporal behavior of the DSD and to directly investigate the
28 conditions favorable to the onset of the EDSD in natural rain. We exploited a large disdrometer
29 dataset collected in the framework of the Ground Validation activities related to the NASA Global
30 Precipitation Measurement mission. More than 200,000 one-minute data of two-dimensional video
31 disdrometer (2DVD) are collected over USA to represent a wide range of precipitation types. The
32 original data are averaged over 2 minutes and an automatic algorithm is used on a selected subset
33 to identify samples with EDSD. Results show that the EDSD occurs mainly in convective events and
34 lasts for very short time intervals (2 to 4 minutes). It is more frequent for rain rate between 20 and
35 40 mm h⁻¹ and it mostly occurs during sharp increase of precipitation rates.

36

37

38

39

40

41

42

43

44

45	Keywords
46	Equilibrium Drop Size Distribution
47	Time evolution
48	Collisional breakup
49	Breakup detection algorithm
50	Radarmeteorology
51	

52 1. Introduction

53

54 The Drop Size Distribution (DSD) is a fundamental property of precipitation and is widely
55 investigated through laboratory, numerical modeling and field studies. A detailed knowledge of DSD
56 structure and variability is required in remote sensor based precipitation retrieval algorithms (Tokay
57 et al., 2016), in cloud resolving models (Tao et al. 2014) and in application to soil science and
58 agriculture (Caracciolo et al, 2012).

59 From the cloud microphysics point of view, the DSD shape at the ground is determined in natural
60 rain by the complex interplay of a number of mechanisms (Radhakrishna and Rao, 2009), where the
61 collisional breakup is known as the process that limits the maximum raindrop size (McTaggart-
62 Cowan and List, 1975; Barros et al., 2010). A large raindrop falling within or below a cloud and
63 colliding with smaller drops, forms a larger raindrop when the Collisional Kinetic Energy (CKE) is
64 lower than a limiting value (about $5 \mu\text{J}$), while larger CKE values indicate that the energy cannot be
65 dissipated by the viscous motions of the merged drop, and the drop breaks up (Low and List, 1982a,
66 Porcù et al., 2013). The drop disruption leads to a number of fragments with a well-defined
67 distribution: one peak at size slightly smaller than the largest colliding drop, and one peak at very
68 small drop size (Low and List, 1982a). Schlottko et al. (2010), who simulated the Low and List (1982a)
69 experiment, found that collisional breakup takes place even for CKE slightly lower than $5 \mu\text{J}$, in cases
70 of grazing collisions.

71 The combined effect of coalescence and collisional breakup has been studied mainly by simulations
72 in numerical models, focusing on the shape variation of the initial DSD up to reach the so-called
73 equilibrium stage, described by the Equilibrium DSD (EDSD). The parameterization proposed by Low
74 and List (1982a,b) of breakup fragments is taken as reference in most of the numerical schemes to
75 simulate DSD evolution in time until the EDSD is reached. While early studies concerning this topic

76 found a three-peak EDSD (Valdez and Young, 1985; Brown, 1988; Feingold et al., 1988; Chen and
77 Lamb, 1994), McFarquhar (2004) derived a different parameterization of the breakup fragments,
78 leading to a different shape of the EDSD with respect to the previous works. Starting from an initial
79 exponential DSD corresponding to 54 mm h^{-1} rainfall rate, the resulting EDSD presents a bi-modal
80 shape with the peaks at 0.26 and 2.3 mm. Prat and Barros (2007), using a discrete model, found that
81 the EDSD has the same shape (bi-modal) independently from the initial DSD and for the same rainfall
82 rate and breakup kernel, with marked difference in the time required to reach the EDSD. In their
83 follow-up studies, deepening the influence of the microphysical processes on Z-R relationship (Prat
84 and Barros, 2009), they found that, in general, for rain rates lower than 20 mmh^{-1} the coalescence
85 is the dominant process. For higher rain rates, the breakup is the dominant process and the time to
86 reach the EDSD is about half as long as in the case of light rainfall (about 30 minutes compared with
87 at least one hour). Moreover, they found that for heavy rain the sensitivity of the DSD shape to the
88 rain rate is negligible. More recently, Prat and Barros, (2012) developed a new parameterization of
89 the fragments of the drop-drop collision leading to EDSD with a lower number of large drops. This
90 evidences that the EDSD can be reached at lower rainfall rate regimes than what they previously
91 found.

92 As also highlighted by McFarquhar (2004), the literature is scant of EDSD observations from natural
93 rain. While the numerical model outputs allow for monitoring rain DSDs resulting from coalescence
94 and breakup events at every time stamp, thus unambiguously assessing the EDSD onset, the
95 detection of EDSD in natural rain is more questionable. Hu and Srivastava (1995) tried to compare
96 their model output with disdrometer observations noticing that in addition to the bi-modal shape,
97 a slope in the large drops tail of observed DSD around 20 cm^{-1} can be taken as a signature of EDSD,
98 shaped by collisional processes. However, this result could be affected by the known problem of
99 Joss Waldvogel disdrometer in detecting large drops.

100 A further characteristic of the EDSD is the bi-modality. Porcù et al. (2013, 2014) observed bi-modal
101 DSD shape from measurements at different altitudes using a low power X-band Doppler
102 disdrometer. The position of the DSD peaks agrees quite well with that obtained by different
103 numerical models, even though there was altitude dependence. Bi-modal DSDs were also observed
104 by Steiner and Waldvogel (1987), Zawadzki and de Agostinho Antonio (1988), List et al. (1988), and
105 Asselin de Beauville et al. (1988), which all used Joss-Waldvogel disdrometer. Willis and Tattelman
106 (1989) also observed bi-modal DSD at very high rainfall rates collected during hurricanes and tropical
107 storms using an optical spectrometer. However, bi-modality does not seem to be a sufficient
108 condition to have EDSD, since other cloud processes are able to produce bi-modal DSD
109 (Radhakrishna and Rao, 2009). Based on both theoretical studies and experimental observations,
110 D’Adderio et al. (2015) developed an automatic algorithm to identify bi-modal DSD (with peaks in
111 well defined diameter ranges) and labeled them as EDSD, analyzing two-minutes samples from six
112 different field campaigns. They found that, in natural rain, the reaching of the EDSD is rare (at most
113 7% of the analyzed samples) and occurs mainly during convective precipitation.

114 In this paper, by using the D’Adderio et al. (2015) algorithm, the conditions favorable to reach the
115 EDSD in natural rain have been studied. To this end, an extensive disdrometer dataset, collected
116 during several field campaigns in the framework of the NASA/JAXA Global Precipitation
117 Measurement Mission (GPM) ground validation (GV) activities, is analyzed to extract EDSD samples
118 in natural rain. The automatic algorithm developed by D’Adderio et al. (2015), based on the slope
119 of the DSD curve between 1.0 and 2.6 mm, is used to select the EDSD samples as collected by the
120 two-Dimensional Video Disdrometer (2-DVD).

121 We remark that the GPM GV field campaigns, although providing a large amount of high quality
122 disdrometric data, were not planned to study DSD properties at cloud scale. A dedicated field
123 campaign would be desirable to complete the results of the present work allowing a lagrangian

124 observation of the cloud to assess the full temporal evolution of the ESD in the same developing
125 cloud column.

126 The paper is organized as follow: Section 2 presents a brief description of the field campaigns
127 characteristics useful to our aim; a critical description of the algorithm to identify the ESD is given
128 in Section 3, while Section 4 and Section 5 describe the overall results obtained and some case study,
129 respectively. The last section provides the conclusions.

130

131

132 2. Field Campaigns characteristics

133

134 This study uses the 2DVD (Schönhuber et al. 2007) observations from five different field campaigns
135 of the GPM-GV program: Iowa Flood Studies (IFloodS – 41.6N, 91.5W from May 1 to June 15, 2013),
136 Midlatitude Continental Convective Clouds Experiment (MC3E – 36.7N, 97.1W from April 22 to June
137 6, 2011), Wallops Flight Facility (Wallops – 37.5N, 75.5W from July 22, 2013 to October 7, 2015 not
138 continuously), Integrated Precipitation and Hydrology Experiment (IPHEX – 35.5N, 82.5W from May
139 1 to June 15, 2014) and Alabama-Huntsville (Alabama – 35N, 87W from December 17, 2009 to
140 October 13, 2011). The drop-by-drop raw output of the 2DVD was binned in 0.2 mm bin width and
141 averaged over two minutes, called samples hereafter. Table 1 summarizes the characteristics of
142 2DVD observations relevant for our analysis in each field campaigns. The rightmost column reports
143 the samples with positive Highest Slope (HS), which is the maximum slope of the linear fit of the
144 DSD between 1.0 and 2.6 mm, defined in D’Adderio et al. (2015) that will be discussed in the next
145 Section.

146

Field Campaign	Events	Samples	Stratiform Samples	Convective Samples	HS>0 Samples
Alabama	4	68		68	7
IFloodS	28	1016	63	953	48
IPHEX	14	368		368	28
MC3E	10	174		174	13
Wallops	75	1466	31	1435	133

147 Table 1. Characteristics of the dataset.

148

149 The number of rainfall events considered in the present work ranges from 4 for the Alabama dataset
150 to 75 for the Wallops site (Table 1). An event is defined as set of at least 8 samples with rain rate
151 exceeding 1 mm h^{-1} and reporting at least one EDSD selected according to the D'Adderio et al. (2015)
152 algorithm. This has been considered a good compromise between having a sufficient time interval
153 to follow the evolution of the precipitation, and to include stratiform precipitation that could lead
154 to EDSD. Each event is identified as convective or stratiform according to Bringi et al. (2003): the
155 classification is based on the standard deviation of the rain rates. If the standard deviation of the
156 rain rates is $\geq 1.5 \text{ mmh}^{-1}$, then the event is considered convective otherwise it is considered
157 stratiform. Ioannidou et al. (2016) used the same criterion to validate the measurements of the
158 Precipitation Radar (PR) of the Tropical Rainfall Measuring Mission (TRMM) by comparing the
159 rainfall estimates with 2DVD and X-band ground based radar measurements. Several authors
160 conducted studies about the development of technique to characterize convective and stratiform
161 precipitation. Among the others, Caracciolo et al. (2006) based their analysis using high order DSD
162 moments, while Thurai et al. (2016) developed a separation technique in the N_w - D_0 space. Table 1
163 also shows that almost all the selected samples are classified as convective, while the last column
164 reports the number of samples with EDSD occurrence.

165 Table 2 reports, for each dataset, the number of all registered convective and stratiform episodes,
166 considered just as set of at least 8 samples with rain rate exceeding 1 mm h^{-1} regardless if EDSD is
167 present or not. The percentage of episodes with EDSD (previously defined as event) ranges between

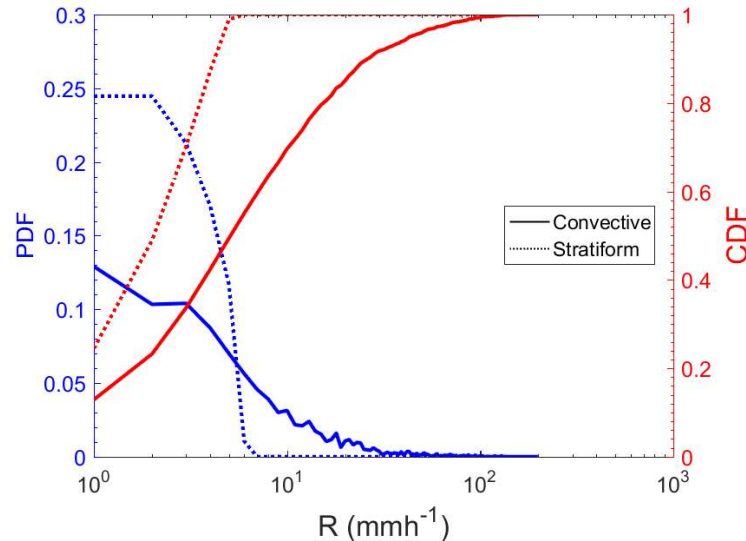
168 17 and 27% of cases selected according to our classification. All the datasets report a significant
 169 number of stratiform episodes, even if only three present at least one EDSO sample. This aspect
 170 highlights the strict relationship between the onset of EDSO and the convective precipitation.

Field Campaign	All Convective	Convective with EDSO	All Stratiform	Stratiform with EDSO
Alabama	15	4	12	0
IFloodS	143	26	123	2
IPHEX	80	14	33	0
MC3E	54	10	54	0
Wallops	154	74	212	1

171 Table 2. Convective/stratiform classification for the registered episodes.

172

173 Figure 1 shows the Probability Density Function (PDF – blue lines) and Cumulative Density Function
 174 (CDF – red lines) of rain rate for the considered events (3,092 samples) after the
 175 convective/stratiform discrimination (solid/dashed lines).



176 Figure 1. PDF (blue lines) and CDF (red lines) for convective (solid lines) and stratiform (dashed lines)
 177 samples.

178 The rain rate of the stratified events presents a narrow distribution and never exceeds 7 mm h^{-1}
 179 with a marked peak around 2 mm h^{-1} . The PDF of the convective events is toward higher values, up
 180 to more than 100 mm h^{-1} , and about the 30% of the samples has rain rate exceeding 10 mm h^{-1} .

181

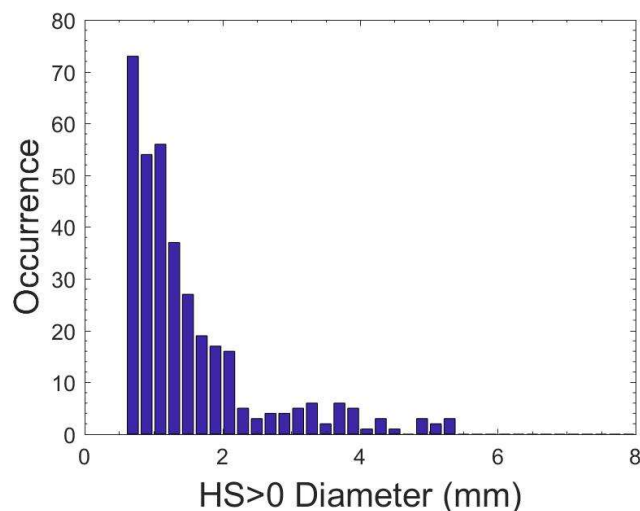
182 3. Equilibrium Drop Size Distribution detection algorithm

183 Following laboratory experiment results (Low and List, 1982a, b) and numerical modeling output
184 (Prat and Barros, 2012), the EDSD bi-modal shape is characterized by: 1) a peak at very small drops
185 end (around 0.3 mm) due to the breakup fragments; 2) a depletion in the region between 1.0 and
186 1.5 mm due to the drops involved in the collisions; 3) a relative secondary maximum around 2.0
187 mm. This is well observed in numerical simulations, where the EDSD shape is reached after a given
188 time following the start of precipitation, and lasts indefinitely until a modification in the boundary
189 conditions occurs (Prat and Barros, 2009).

190 An automated algorithm based on the slope (HS) of the linear fit of the DSD between 1.0 and 2.6
191 mm has been introduced to identify and select the EDSD in natural rain (D'Adderio et al, 2015). The
192 EDSD is present if the sample satisfies the condition $HS > 0$, i.e. the DSD shape shows the same
193 features found in EDSD obtained by numerical modeling and laboratory experiments. This algorithm
194 is applied to the samples with rain rate exceeding 5 mmh^{-1} , and the events where at least one
195 sample has $HS > 0$ have been selected for further processing.

196 As a matter of fact, the algorithm selects the DSD with positive slope between 1 and 2.6 mm in the
197 diameter spectrum, which have been labeled as EDSD (D'Adderio et al, 2015). We are aware that
198 other mechanisms can induce bi-modality in DSD: size sorting (related to updraft and vertical wind
199 shear or to the beginning of the precipitation), coexistence of melted snowflakes and supercooled
200 droplets, rainshafts overlapping, and any combination of these (Radhakrishna and Rao, 2009). It is
201 difficult, if not impossible, to assess the contribution of each mechanism by analyzing the DSD shape
202 in natural rain. We based the reliability of the results of the algorithm in identifying the EDSD on the
203 correspondence with numerical studies and the discussion below.

204 In order to quantify the possible influence of the above-mentioned mechanisms in the ESD
205 selection, the detection algorithm has been applied to a wider diameter spectrum, between 0.6 and
206 5.0 mm, seeking for $HS > 0$. We found 352 DSD samples, distributed with the size of the point
207 corresponding to $HS > 0$ as shown in Figure 2. For most of the selected DSD (180; 51%) this point is in
208 the interval 1.0-2.6 mm, a large fraction (127; 36%) is between 0.6-1.0 and the reminders (45; 13%)
209 are distributed above 2.6 mm. Most of the DSD with positive HS in the interval 0.6-1.0 mm are not
210 bi-modal but can be due to the underestimation of small drops by 2DVD (Tokay et al. 2013) resulting
211 in a peak between 0.5 and 1.0 mm. The rest of the graph shows that positive HS can be found along
212 the diameter spectrum for all values, but its occurrence is much more frequent in the 1.0-2.6
213 interval. This analysis, in our view, supports our hypothesis of labeling as ESD the DSD with positive
214 HS in this interval, since the other mentioned mechanisms producing bi-modal DSD are expected to
215 be distributed randomly without any preferential size. Even if we are confident that the DSD with
216 positive HS in the interval 1.0-2.6 mm are ESD, we cannot exclude a marginal contamination from
217 DSD for which bi-modality is not due to equilibrium.



218 Figure 2. Distribution of drop diameter corresponding to $HS > 0$ when the identification algorithm
219 (D'Adderio et al., 2015) is applied to 0.6-5 mm range.

220

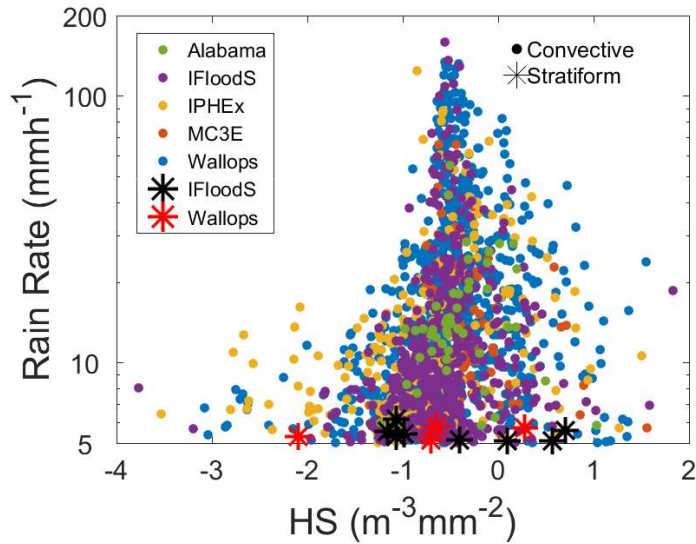
221 Several arguments makes the effects of sorting unlikely in shaping the DSD: 1) the 2DVD sampling
222 volume is rather small (around 11 m^3 for largest drops), and thus making influences of size sorting
223 in rain volumes unlikely, as it is more common in radar data (Dawson et al., 2015); 2) generally size
224 sorting DSD presents a marked peak for large drops (2 mm of diameter or more), and with few drops
225 at small size (Kumjian and Ryzhkov, 2012). Among the 352 DSD only 18 show a signal that can be
226 due to size sorting contamination, with the peak at larger size (above 1.3 mm) higher than the peak
227 at smaller drop size, while we never observed DSD with single peak at diameters larger than 2 mm.
228 Finally, the possible contamination from DSD shaped by the coexistence of melted ice flakes and
229 supercooled drops (or other anomalous distribution of frozen hydrometeors aloft) is unlikely, given
230 the fact that the freezing level during the considered events is always higher than 2500 m a.s.l..

231

232 4. Results

233 A first analysis was devoted to assess the occurrence of EDSD in convective and stratiform events:
234 Figure 3 shows each sample according to its rain rate and HS value. EDSD occurrence in stratiform
235 events is very rare and only three events in IFloodS and Wallops datasets (see Table 2) reported only
236 three samples with EDSD (i.e. $HS > 0$). The rain rate of the EDSD (i.e. $HS > 0$) ranges mainly between 5
237 and 70 mm h^{-1} , while at higher rain rates, even exceeding 100 mm h^{-1} , the HS values is centered
238 around $-0.5 \text{ mm}^{-3}\text{m}^{-2}$. In general, higher rain rates have lower HS values even if positive, while lower
239 rain rates can reach HS values larger than one, indicating a marked two-peak DSD.

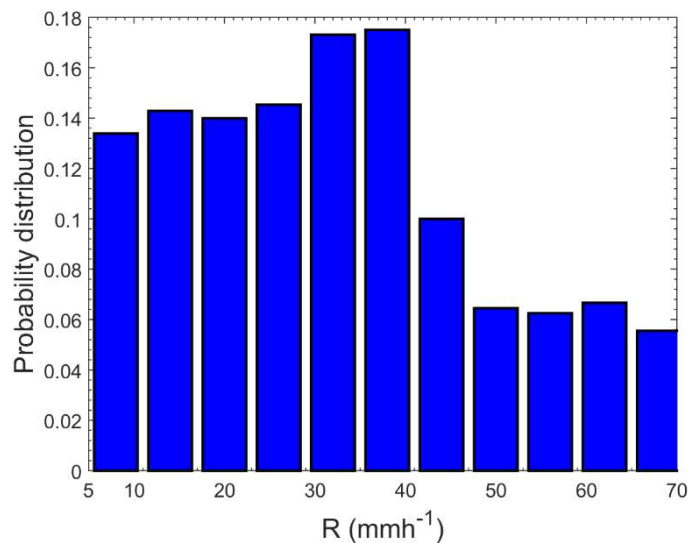
240



241 Figure 3. Distribution of the samples belonging to the selected events according to their rain rate
 242 and HS. Dots indicate convective samples, while stars indicate stratiform samples.

243 The dependence of ESD occurrence on the rain rate is presented by considering the fraction of
 244 ESD samples as function of the rain rate sampled over 6 mm h⁻¹ wide intervals (Figure 4). The
 245 fractional occurrence of ESD slightly increases with the rainfall rate to reach a maximum above
 246 17% around 40 mm h⁻¹, while the probability to have ESD decreases below 10% at higher rain rates.

247



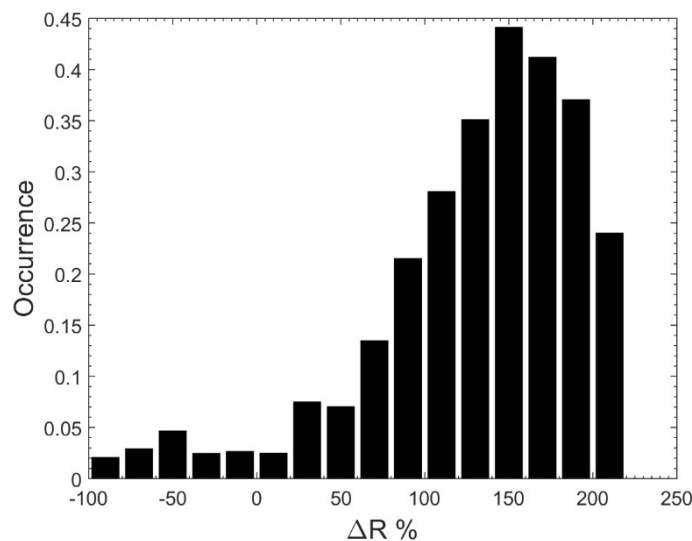
248 Figure 4. Fractional occurrence of samples with ESD (HS>0) as function of the corresponding rain
 249 rate.

250 The onset of EDSO seems to be weakly related to rainfall intensity above the threshold used. To
251 assess if the EDSO is sensitive to the change of the rainfall intensity, the percent rain rate difference
252 between two consecutive samples is calculated and, for each value, the percentage of samples with
253 EDSO is reported at 20% intervals (Figure 5). Results indicate that a sudden increase of precipitation
254 rate (especially between 100 and 200%) is favorable to the occurrence of EDSO. The samples where
255 the rainfall rate increases between 120 and 200% have the probability higher than 30% to have
256 EDSO, with a peak of 45% for a relative increase of rain rate of 150%. A sudden decrease of rainfall
257 rate between two consecutive samples, shows a very low occurrence (about 2%) of EDSO, as well
258 very large positive rain rate variation (above 220%) does not present any EDSO.

259

260

261

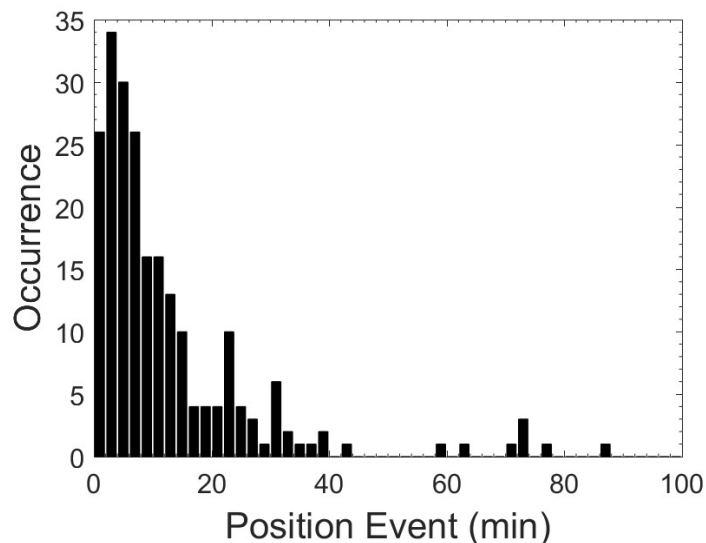


262 Figure 5. Fractional occurrence of samples with $HS > 0$, as function of the relative rain rate difference
263 between each sample and the previous one.

264

265 A further analysis has been devoted to understand how the DSD evolves in time to reach the
266 equilibrium stage. The delay (in minutes) between the first rain detection for each event and the
267 appearance of the ESD is computed for all the dataset (Figure 6). Each bar is two-minutes width
268 and it is centered in the middle value of the class (i.e. the first bar is centered at minute one and
269 indicated the detection of ESD at first or second minute of the considered event).

270 The distribution is clearly peaked for time delays between 2 and 8 minutes after the precipitation
271 is first detected: for the 80% of the ESD observation, it takes place within 20 minutes from the
272 start of the event observation, and in the 10% of the cases, the ESD coincides with the first
273 observation of the event. There are also very few events for which the ESD takes place after a long
274 time (between 60 and 90 minutes). ESD was observed only once in an event in most of the
275 observations (75%), while two consecutive ESD samples were present only in the 6% of the time.
276 Longer period with ESD continuously detected are even rarer: 10 and 2 times (around 4 and 1% of
277 the ESD samples) for 3 and 4 consecutive ESD, respectively. Moreover, in the 15% of the cases
278 ESD appears two or more times (not consecutively) in different stages of the same event.



279 Figure 6. Number of samples with $HS > 0$ as function of the time difference with respect to the first
280 observation of the event (i.e. $RR > 1 \text{ mm h}^{-1}$).

281

282 With our observing system (fixed and point-like measurements), however, we are not able to follow
283 separately the spatial and time evolution of the same cloud column, and thus we cannot
284 unambiguously assess the time needed to a given cloud column to reach the EDS. This limitation
285 prevents a deeper analysis of the results, and we discussed EDS properties not affected by the
286 inadequacy of the experimental settings. A field measurement designed for this purpose, however,
287 would require a very high density disdrometers network with a focused spatial distribution and a
288 dedicated radar with a high temporal resolution (given the fast response of the transient EDS) to
289 follow the evolution of the precipitation pattern.

290

291 5. Case studies

292 Times series of rain rate and HS are presented for three cases: two illustrate how the EDS is
293 reached in convective cases, and one will describe a stratiform case where the EDS is not reached
294 despite its long duration.

295 5.1 Convective events

296 The convective events selected show at least one EDS spectrum during their lifetime. The time
297 evolution of HS can be explained according to the time of observation of the EDS occurrence with
298 respect to the rain rate peak and the start of the observation. The analysis leads to the division of
299 the selected events in two main groups.

300 For the events belonging to the first group, rainrate is already high at the first observation, and the
301 HS is positive in one of the first samples: in more than 10% of the cases (Figure 6), the first sample
302 observed in an event has a relatively large positive HS value, indicating that the EDS is found in
303 proximity of the edge of the rain pattern at the beginning of the rain event observation. We interpret

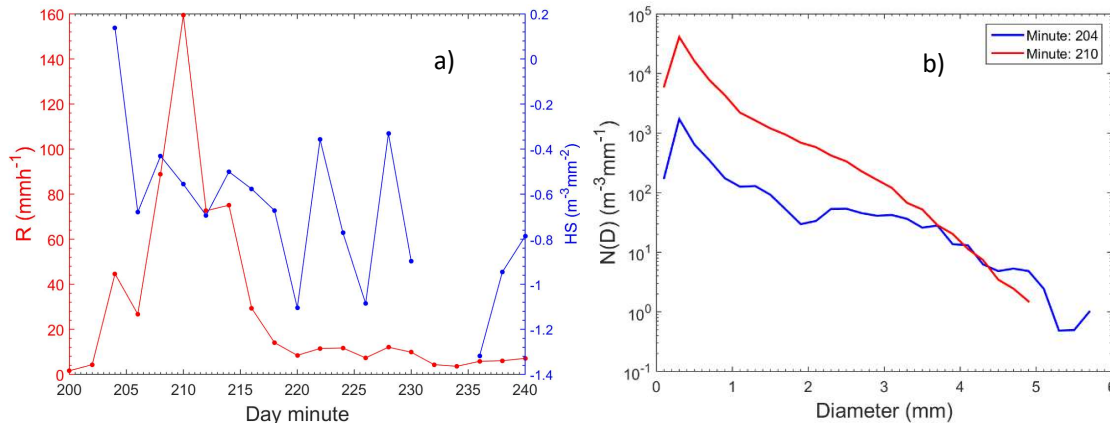
304 this behavior as follows: the rain system overpasses the instrument when the rain column already
305 reached a mature stage. Often rain rate keeps increasing with time while HS drops below zero,
306 indicating that the EDSD is lost due to the passage of the most intense part of the weather system
307 over the instrument.

308 The second group of events is characterized by light/moderate rain rate and negative HS value at
309 the beginning of the observation, rain rate increases more slowly with time, and reaches maximum
310 values within 15-25 minutes after the first observation. HS increases in parallel with rain rate,
311 reaching a positive value in correspondence with the maximum rain rate. We observe, in this case,
312 the transition between negative and positive HS values, related to the increase of rain rate.

313 We present two case studies to illustrate the first and second group.

314 The event occurred on October 20, 2013 during the IFloodS field campaign is an example of well-
315 defined convective event, belonging to the first group, where rain rates reached 160 mm h^{-1} (Figure
316 7a). Measured rain rate increased from 4 to 44 mm h^{-1} in two minutes, and the first positive HS value
317 was found by the algorithm at minute 204. The HS then dropped down below zero indicating that
318 the EDSD signal was lost while rain rate further increased, and HS oscillates around $-0.5 \text{ m}^{-3}\text{mm}^{-2}$
319 after the peak rain rate ($R = 159 \text{ mm h}^{-1}$) at minute 210. A close inspection of the DSD of minute 204
320 and minute 210 (Figure 7b), shows an EDSD with a marked depletion of drops around 2 mm, that
321 evolves to a DSD with much more drops until 4.5 mm and a well-defined slope. However, a weak
322 change of concavity is present between 1 and 3 mm, indicating that other processes (Radhakrishna
323 and Rao 2009), occurring during such intense episodes, affect the equilibrium between breakup and
324 coalescence, and prevent the maintenance of the EDSD.

325



326

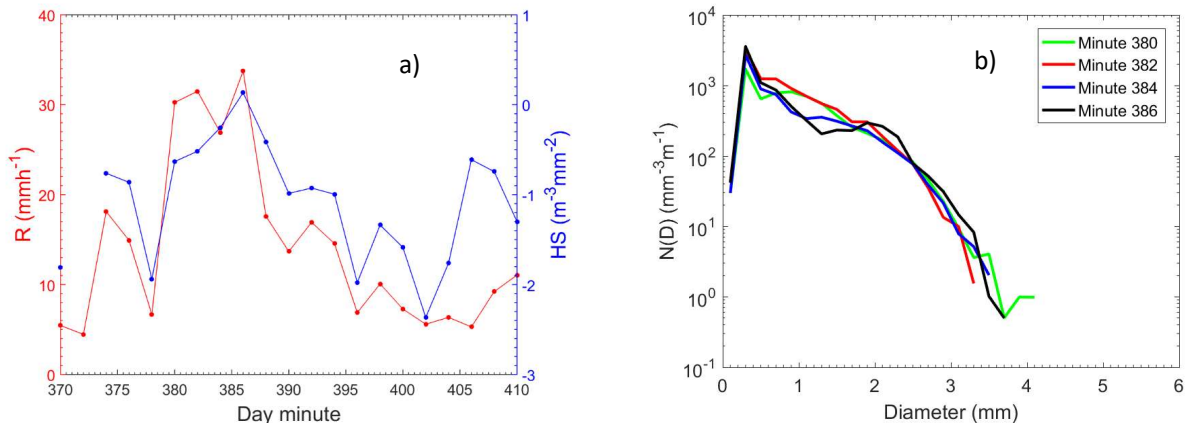
327 Figure 7. a) Time series of rain rate (red dot-line) and HS (blue dot-line) values, and b) DSDs of two
 328 samples of a rain event occurred on May 20, 2013 during IFloodS field campaign.

329

330 A second convective case, occurred on May 15, 2014 during the IPHEX field campaign, is reported
 331 to represent the second groups of events. In this case, HS reached its positive value at the peak of
 332 rain rate. The HS constantly increases from the beginning of the observation (except for one sample
 333 where a marked decrease of HS is related to a marked decrease of rain rate), up to reach a positive
 334 value. The precipitation peak reaches lower value with respect to the previous case, and this is a
 335 general difference between the two groups: the average peak intensity is 60.6 mmh^{-1} and 36.3 mm
 336 h^{-1} for the first and the second group, respectively. On the other hand, the mean rain rate of the
 337 EDSD samples does not show any difference for the two groups, with 14.8 and 13.8 mmh^{-1} for the
 338 first and second group, respectively. The higher rain rates do not seem support the developing and
 339 maintaining of EDSD. Furthermore, this case also confirms the transient nature of the EDSD, with its
 340 extremely short duration (only one sample).

341 The analysis of the DSD (Figure 8b) shows a clear transition from a well-defined Gamma distribution
 342 shape at minute 380 (green line) and at minute 382 (red line), both with μ parameter around 4.8, to
 343 a bi-modal shape indicating the EDSD occurrence. Minute 384 (blue line) evidences the breakup
 344 effects with a concavity change already present leading to EDSD at minute 386 (black line).

345



346

347 Figure 8. a) The same of Figure 6a, but for the event occurred on May 15, 2014 during IPHEX field

348 campaign; b) DSDs preceding the equilibrium stage and EDSD.

349

350 5.2 Stratiform episode

351 The time evolution of rain rate and HS is shown for a stratiform case, occurred on December 29,

352 2013 at Wallops Island, Virginia, not classified as event since HS never reaches positive values (Figure

353 9). This case was observed for more than one hour and the rain rate was between 5 and 10 mm h^{-1} .

354 The HS parameter at the beginning of the observation had high negative value, indicating a very

355 steep DSD, with a relatively large amount of small drops and no drops with diameter larger than 2

356 mm. The HS increases rapidly, indicating the formation of larger drops, as effect of coalescence, and

357 then keeps increasing slowly with time, reaching the highest value after 60 minutes of nearly

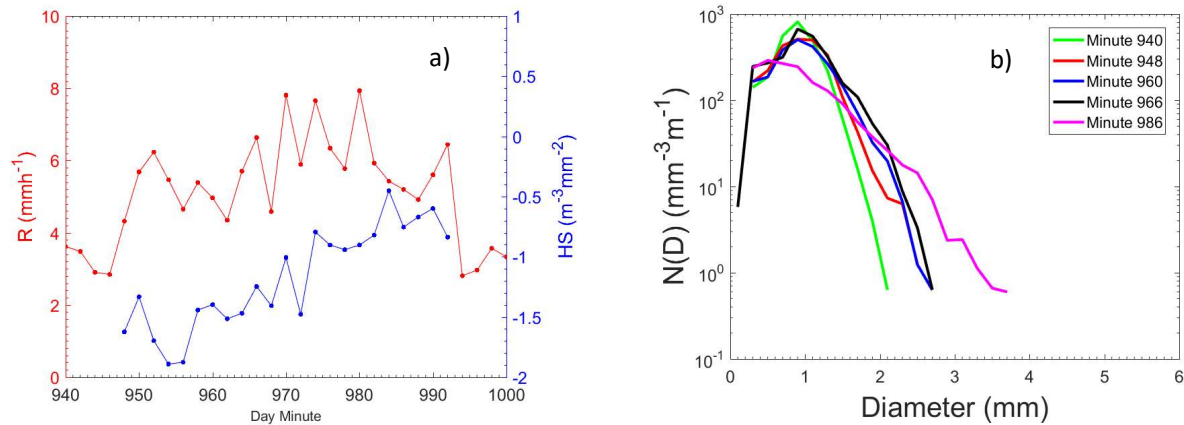
358 constant rain intensity, still lower than zero (Figure 9a). This shows that along the event the DSD

359 modifies, reducing the slope of the curve between 1.0 and 2.6 mm. Comparing our results with Prat

360 and Barros (2009) numerical simulations, this case demonstrates that time necessary to reach the

361 EDSD during a stratiform event could be much longer with respect to a convective event.

362 The DSD of the considered event does not present any particular characteristic (Figure 9b). The
363 measured drop diameters are generally lower than 3.5 mm, well below the breakup size (Porcù et
364 al, 2013), therefore no bi-modal shape can be identified within this event.



365

366 Figure 9. a) The same of Figure 6a, but for December 29, 2013 at Wallops Island, Virginia; b) sampling
367 of DSDs for the whole period of observation.

368

369 Conclusions

370 High density, high quality disdrometric datasets have been analyzed to investigate the DSD
371 dynamics in natural rain. A specific algorithm developed to identify bi-modal DSD is applied to more
372 than 6,000 minutes of liquid precipitation 2DVD measurements collected in different seasons and
373 locations. We propose a number of arguments to assess that these bi-modal DSD are EDSD, allowing
374 the analysis of their temporal characteristics.

375 Our results demonstrate that EDSD is reached almost exclusively in convective rain (128 convective
376 events and 3 stratiform events), and confirm that the onset of EDSD is a rare event in natural rain
377 (Prat and Barros, 2012) occurring at most around 7% of the times (D'Adderio et al., 2015).

378 We found that EDSD shows up few minutes after the start of the observation (about 66% in the first
379 10 minutes), indicating that EDSD is more likely to take place in the proximity of the external edge
380 of the rain area. Since most of the considered events have a total duration of around 20-30 minutes,
381 thus, we can extrapolate that the onset of the EDSD is expected to take place 10-15 minutes after
382 the beginning of the precipitation, confirming the time scales suggested by numerical modeling.

383

384 A second relevant feature is the short lifetime of the EDSD, observed in only one 2-minute sample
385 in most of the cases (about 75% of the cases). EDSD, moreover, is often detected in cases of
386 relatively rapid precipitation rate increase. The probability to have an EDSD exceeds 25% for those
387 samples presenting a rain rate increase of more than 100% with respect to the previous sample,
388 with a relative maximum higher than 45% of EDSD occurrence when the fractional increase of rain
389 rate is around 150%. In the case of the maximum rain rate observed is very high (above 50 mm h^{-1})
390 the EDSD signal is lost, due to a number of mechanisms of higher order of complexity with respect
391 to the coalescence-breakup balance (Radhakrishna and Rao 2009). If the rainfall rate remains limited
392 below 50 mm h^{-1} , is more frequent to find the EDSD in correspondence to the maximum rain rate.

393 For a group of events the instrument does not observe the precipitation onset: at a certain stage of
394 the precipitation column life, the system reaches the instrument (we deducted this since the first
395 sample presented high rain rate values) and the measurement starts from the external part of the
396 rain column, where EDSD is detected. For a second group of events, the instrument observes the
397 early stages of precipitation development until a maximum rain rate is reached: HS growths with
398 rain intensity (starting from very low values) and maximum rainrate and EDSD are observed at the
399 same time. In case of stratiform episodes, the DSD changes in time, increasing the drop size, but
400 reaches equilibrium in only three cases.

401 The observation of the time evolution of DSD in natural rain is a difficult task, since it would need
402 Lagrangian measurements of the cloud column. With our Eulerian approach, however, we assess
403 some basic properties of the onset of the ESD, compatible with numerical modeling and laboratory
404 results. The results and related comments we reported in this work would be confirmed by an ad
405 hoc experimental campaign, which seems, however, difficult to design and carry on.

406

407 Acknowledgements

408 This study was partially funded by the “The Foundation BLANCEFLOR Boncompagni Ludovisi, née
409 Bildt”. Thanks to Patrick N. Gatlin of NASA Marshall Space Flight Center and Matthew Wingo of the
410 University of Alabama at Huntsville for maintenance of 2DVD during NASA Global Precipitation
411 Measurement (GPM) mission ground validation field campaigns led by Walter Petersen of NASA
412 Wallops Flight Facility.

413

414 References

415 Barros, A. P., Pratt O. P., and Testik F. Y., 2010: Size distribution of raindrops. *Nat. Phys.*, 6, 232.

416

417 Bringi V.N., Chandrasekar V., Hubbert J., Gorgucci E., Randeu W. L., and Schoenhuber M., 2003:
418 Raindrop Size Distribution in Different Climatic Regimes from Disdrometer and Dual-Polarized Radar
419 Analysis. *J. Atmos. Sci.*, 60, 354–365.

420

421 Brown, P. S., Jr., 1988: The effects of filament, sheet, and disk breakup upon the drop spectrum. *J.*
422 *Atmos. Sci.*, 45, 712–718, doi: 10.1175/1520-0469(1988)045<0712:TEOFSA>2.0.CO;2.

423

424 Caracciolo, C., Prodi, F., Battaglia, A., Porcù, F., 2006. Analysis of the moments and parameters of a
425 gamma DSD to infer precipitation properties: a convective stratiform discrimination algorithm.
426 Atmos. Res. 80 (2–3), 165–186.

427

428 Caracciolo, C., Napoli M., Porcù F., Prodi F., Dietrich S., Zanchi C. and Orlandini S., 2012: Raindrop
429 size distribution and soil erosion. J. Irrig. Drain Eng., 138, 461-469.

430

431 Chen, J.-P. and Lamb D., 1994: Simulation of Cloud Microphysical and Chemical Processes Using a
432 Multicomponent Framework. Part I: Description of the Microphysical Model. J. Atmos. Sci., 51,
433 2613-2630, DOI: [http://dx.doi.org/10.1175/1520-0469\(1994\)051<2613:SOCMAC>2.0.CO;2](http://dx.doi.org/10.1175/1520-0469(1994)051<2613:SOCMAC>2.0.CO;2).

434

435 D’Adderio L.P., Porcù F. and Tokay A., 2015: Identification and analysis of collisional break-up in
436 natural rain. J. Atmos. Sci., 72, 3404-3416, DOI: 10.1175/JAS-D-14-0304.1.

437

438 Dawson, D.T. II, Mansell, E.R. and Kumjian, M.R., 2015: Does wind shear cause hydrometeor size
439 sorting, J. Atmos. Sci., 72, 340-348

440

441 Feingold G., Tzivion (Tzitzvashvili) S. and Leviv Z., 1988: Evolution of Raindrop Spectra. Part I:
442 Solution to the Stochastic Collection/Breakup Equation Using the Method of Moments. J. Atmos.
443 Sci., 45, 3387-3399, DOI: [http://dx.doi.org/10.1175/1520-0469\(1988\)045<3387:EORSPI>2.0.CO;2](http://dx.doi.org/10.1175/1520-0469(1988)045<3387:EORSPI>2.0.CO;2)

444

445 Ioannidou M.P., Kalogiros J.A., Stavrakis A.K., 2016: Comparison of the TRMM Precipitation Radar
446 rainfall estimation with ground-based disdrometer and radar measurements in South Greece.

447 Atmos. Res., 181, 172-185, DOI: <http://dx.doi.org/10.1016/j.atmosres.2016.06.023>

448

449 Kumjian M.R. and Ryzhkov A.V., 2012: The Impact of Size Sorting on the Polarimetric Radar
450 Variables. *J. Atmos. Sci.*, 69, 2042-2060. DOI: 10.1175/JAS-D-11-0125.1

451

452 Low, T. B., and List R., 1982a: Collision, coalescence and breakup of raindrops. Part I: Experimentally
453 established coalescence efficiencies and fragment size distributions in breakup. *J. Atmos. Sci.*, 39,
454 1591–1606, doi:10.1175/1520-0469(1982)039,1591:CCABOR.2.0.CO;2.

455

456 Low, T. B., and List R., 1982b: Collision, coalescence and breakup of raindrops. Part II:
457 Parameterizations of fragment size distributions. *J. Atmos. Sci.*, 39, 1607–1618, doi:10.1175/ 1520-
458 0469(1982)039,1607:CCABOR.2.0.CO;2.

459

460 McFarquhar G. M., 2004: A new representation of collision-induced breakup of raindrops and its
461 implications for the shapes of raindrop size distributions. *J. Atmos. Sci.*, 61, 777–794.

462

463 McTaggart-Cowan, J.D. and List R., 1975: Collision and breakup of water drops at terminal velocity.
464 *J. Atmos. Sci.*, 32, 1401–1411.

465

466 Porcù, F., D'Adderio L. P., Prodi F. and Caracciolo C., 2013, Effects of altitude on maximum raindrop
467 size and fall velocity as limited by collisional breakup, *J. Atmos. Sci.*, 70, 1129-1134.

468

469 Porcù, F., D'Adderio L. P., Prodi F. and Caracciolo C., 2014, Rain drop size distribution over the
470 Tibetan Plateau, *Atmos. Res.*, 150, 21-30.

471

472 Prat, O. P. and Barros A. P., 2007: A Robust Numerical Solution of the Stochastic Collection–Breakup
473 Equation for Warm Rain. *J. App. Meteor. Climatol.* 46, 1480-1497.

474

475 Prat, O. P. and Barros A. P., 2009: Exploring the transient behavior of Z-R relationships-Implications
476 for Radar Rainfall Estimation. *J. Applied Meteor. and Clim.*, 48, 2127-2143.

477

478 Prat, O. P., Barros A. P. and Testik F., 2012: On the influence of raindrop collision outcomes on
479 equilibrium size distributions. *J. Atmos. Sci.*, 69, 1534–1546, doi:10.1175/JAS-D-11-0192.1.

480

481 Radhakrishna, B., and Rao T. N., 2009: Statistical characteristics of multipeak raindrop size
482 distributions at the surface and aloft in different rain regimes. *Mon. Wea. Rev.*, 137, 3501–3518,
483 doi:10.1175/2009MWR2967.1.

484

485 Schlottko, J., Straub W., Beheng K., Goma H., and Weigand B., 2010: Numerical investigation of
486 collision-induced breakup of raindrops. Part I: Methodology and dependencies on collision energy
487 and eccentricity. *J. Atmos. Sci.*, 67, 557–575, doi:10.1175/2009JAS3174.1.

488

489 Schönhuber, M., Lammer G., and Radeu W. L., 2007: One decade of imaging precipitation
490 measurement by 2Dvideo-disdrometer. *Adv. Geosci.*, 10, 85–90, doi:10.5194/adgeo-10-85-2007.

491

492 Steiner, M. and Waldvogel A., 1987: Peaks in Raindrop Size Distributions. *J. Atmos. Sci.*, 44, 3127-
493 3133, DOI: [http://dx.doi.org/10.1175/1520-0469\(1987\)044<3127:PIRSD>2.0.CO;2](http://dx.doi.org/10.1175/1520-0469(1987)044<3127:PIRSD>2.0.CO;2).

494

495 Tao, W.-K., Lang S., Zeng X., Li X., Matsui T., Mohr K., Posselt D., Chern J., Peters-Lidard C., Norris
496 P.M., Kang I.-S., Choi E., Hou A., Lau K.-M. and Yang Y.-M., 2014: The Goddard Cumulus Ensemble
497 model (GCE): Improvements and applications for studying precipitation processes. *Atmos. Res.*, 143,
498 392–424

499 Thurai M., Gatlin P.N., Bringi V.N., 2016. Separating stratiform and convective rain types based on
500 the drop size distribution characteristics using 2D video disdrometer data. *Atmos.Res.*, 169, 416-
501 423. DOI: <http://dx.doi.org/10.1016/j.atmosres.2015.04.011>

502

503 Tokay, A., W. A. Petersen, P. Gatlin, and M. Wing, 2013: Comparison of raindrop size distribution
504 measurements by collocated disdrometers. *J. Atmos. Oceanic Technol.*, 30, 1672-1690.

505

506 Tokay, A., D'Adderio L.P., Wolff D. B. and Petersen W. A., 2016: A Field Study of Pixel-Scale Variability
507 of Raindrop Size Distribution in the Mid-Atlantic Region. *J. Hydrometeo.*, 17, 1855-1868, DOI:
508 <http://dx.doi.org/10.1175/JHM-D-15-0159.1>.

509

510 Valdez, M. P., and Young K. C., 1985: Number fluxes in equilibrium raindrop populations: A Markov
511 chain analysis. *J. Atmos. Sci.*, 42, 1024–1036, doi:10.1175/1520-
512 0469(1985)042<1024:NFIERP>2.0.CO;2.

513

514 Willis, P. T., and Tattelman P., 1989: Drop-size distributions associated with intense rainfall. *J. Appl.*
515 *Meteor.*, 28, 3–15, doi:10.1175/1520-0450(1989)028<0003:DSDAWI>2.0.CO;2.

516

517 Zawadzki, I., and De Agostinho Antonio M., 1988: Equilibrium raindrop size distributions in tropical
518 rain. *J. Atmos. Sci.*, 45, 3452–3459, doi:10.1175/1520-0469(1988)045<3452:ERSDIT>2.0.CO;2.

520 Captions

521 Figure 1. PDF (blue lines) and CDF (red lines) for convective (solid lines) and stratiform (dashed lines)
522 samples.

523

524 Figure 2. Distribution of drop diameter corresponding to $HS > 0$ when the identification algorithm
525 (D'Adderio et al., 2015) is applied to 0.6-5 mm range.

526

527 Figure 3. Distribution of the samples belonging to the selected events according to their rain rate
528 and HS. Dots indicate convective samples, while stars indicate stratiform samples.

529

530 Figure 4. Fractional occurrence of samples with ESD ($HS > 0$) as function of the corresponding rain
531 rate.

532

533 Figure 5. Fractional occurrence of samples with $HS > 0$, as function of the relative rain rate difference
534 between each sample and the previous one.

535

536 Figure 6. Number of samples with $HS > 0$ as function of the time difference with respect to the first
537 observation of the event (i.e. $RR > 1 \text{ mm h}^{-1}$).

538

539 Figure 7. a) Time series of rain rate (red dot-line) and HS (blue dot-line) values, and b) DSDs of two
540 samples of a rain event occurred on May 20, 2013 during IFloodS field campaign.

541

542 Figure 8. a) The same of Figure 6a, but for the event occurred on May 15, 2014 during IPHEX field
543 campaign; b) DSDs preceding the equilibrium stage and EDSD.

544

545 Figure 9 a) The same of Figure 6a, but for December 29, 2013 at Wallops Island, Virginia; b) sampling
546 of DSDs for the whole period of observation.